2013

Terahertz Antenna Phase Shifters Using Integrally-Gated Graphene Transmission-Lines

Pai-Yen Chen
University of Texas at Austin

Christos Argyropoulos
University of Texas at Austin, christos.argyropoulos@unl.edu

Andrea Alu
University of Texas at Austin, alu@mail.utexas.edu

Terahertz Antenna Phase Shifters Using Integrally-Gated Graphene Transmission-Lines

Pai-Yen Chen, *Student Member, IEEE*, Christos Argyropoulos, *Member, IEEE*, and Andrea Alù, *Senior Member, IEEE*

***Abstract*—We propose the concept and design of terahertz (THz) phase shifters for phased antenna arrays based on integrally-gated graphene parallel-plate waveguides (GPPWGs). We show that an active transmission-line may be realized by combining GPPWGs with double-gate electrodes, in which the applied gate voltage can control the guiding properties of the gated sections. This may enable the realization of THz electronic switches and tunable loaded-lines for sub mm-wave antenna systems. Based on these active components, we theoretically and numerically demonstrate several digital and analog phase shifter designs for THz frequencies, with a wide range of phase shifts and small return loss, insertion loss and phase error. The proposed graphene-based phase shifters show significant advantages over other available technology in this frequency range, as they combine the low-loss and compact-size features of GPPWGs with electrically-programmable phase tuning. We envision that these electronic phase shifters may pave the way to viable phased-arrays and beamforming networks for THz communications systems, as well as for high-speed, low-RC-delay, inter/intra-chip communications.**

***Index Terms*—Beam steering, beamforming, graphene, phase shifters, phased-array antennas, terahertz.**

I. Introduction

SEVERAL essential components of microwave antenna systems for telecommunication and radar applications, like phase discriminators, beamforming networks, power dividers, power amplifiers and phased-array antennas are based on electronic phase shifters [1]–[10]. These elements provide the necessary control to electronically steer and reconfigure the radiated beam through phase manipulation of the individual antenna elements, without the necessity of physically repositioning the whole antenna array. A larger number of radiating elements increases the array directivity, but also makes the beamforming network more complex. By reciprocity, a receiving antenna array may be able to select the incoming desired direction of radiation by properly phasing the signals received from each antenna element [1]–[10].

These concepts are well established at radio-frequencies (RF) and microwaves, for which solid-state phase shifters based on PIN diodes or field-effect transistor (FET) switches [10], [11] are widely used. These devices have advantages compared to conventional mechanical or ferrite phase shifters in terms of compact size, integrability with planar circuitry, and high switching speed [10], [11]. However, directly transferring RF phased-arrays to sub mm-wave, THz antenna systems (0.1 THz–10 THz) is very challenging. At these frequencies, conventional active devices, providing electronic control of phase and amplitude, do not offer reliable switching ability [11]. Sandwiched nematic liquid crystals [12] and electrically-driven THz metamaterials [13] have been proposed to realize THz phase shifters or modulators, but they usually require large areas and are difficult to be integrated with planar circuits or on-chip systems. Metamaterial modulators [13] are complicated by the fact that both amplitude and phase, which are strongly frequency dependent, are simultaneously modulated, i.e., the signal amplitude varies with the phase shift. Liquid-crystal-based phase shifters require a high driving potential, up to 125 V, to generate large phase shifts [12].

At the same time, the development of THz antenna technology has seen recent progress, since it may offer greater communication bandwidths and may introduce many exciting applications, such as sensing explosives and biochemical agents, high-resolution through-wall imaging and time-domain spectroscopy [14], [15]. Short-range communications using THz carrier waves [14], [15] also show great commercial potential. Scenarios of interest include on-chip integration of phased-array systems for signal processing or "wireless-on-chip" [6], [16], without the necessity of wired interconnections, leading to substantial improvement in bandwidth, power saving and reliability [6]. Antenna arrays are anticipated to be indispensible components in future sub mm-wave, high-speed wireless communication systems, since their directional radiation properties may lead to less power waste when point-to-point communication is needed.

In general, there are multiple design criteria for RF phase shifters, such as frequency of operation f_0, bandwidth, total phase variation $\Delta\phi$, insertion loss, return loss, switching speed, matching, accuracy, resolution and power consumption [8], [9]. Depending on the specifications and importance of each parameter, various types of RF and microwave phase shifters are currently used. Three general types of phase shifters are considered: switched-line, loaded-line, and reflection-type [8]–[10]. In this paper, we introduce graphene-based antenna technology to realize integrated, electronically controllable phase shifters operating at THz frequencies, to be integrated in sub mm-wave phased antenna arrays. We believe that this technology may be directly applied to broadband communications, sensing and information processing.

Manuscript received May 03, 2012; revised July 25, 2012; accepted August 30, 2012. Date of publication September 24, 2012; date of current version April 03, 2013. This work was supported in part by the U.S. AFOSR with YIP award No. FA9550-11-1-0009 and the ARO grant No. W911NF-11-1-0447.

The authors are with the Department of Electrical and Computer Engineering, University of Texas at Austin, Austin, TX 78712 USA (e-mail: alu@mail.utexas.edu).

Color versions of one or more of the figures in this paper are available online at http://ieeexplore.ieee.org.

Digital Object Identifier 10.1109/TAP.2012.2220327

Graphene is an attractive material in terms of its electronic properties, and the interest around its applications has gained momentum in recent times. Graphene monolayers have been shown to support ultraconfined surface-plasmon polariton (SPP) waves at THz frequencies, with moderate loss and strong field localization and confinement [17]–[20]. These properties have been proposed to realize flatland transformation optics composed of a *one-atom-thick* surface [17], as well as focusing lenses [17], cloaking devices [21] and tunable terahertz metamaterials [22]. In addition, a graphene atomic monolayer can support very high electron (hole) concentrations, due to its large tunability in terms of chemical potential (Fermi energy) μ_c [eV]. Strong attention has been focused on the dramatic change in the complex-valued surface conductivity of graphene $\sigma_s(\omega) = \sigma_s' + j\sigma_s''$ [S] (under an $e^{j\omega t}$ notation adopted throughout this paper) associated to an externally applied bias. This change can be achieved by adjusting to a large degree its chemical potential [17]–[24], either *chemically* by varying the doping profile [20], [25], or *electrically* by biasing external electrostatic field [22], [26] or magnetostatic field via the Hall effect [20]. As a result of the rapid progress in the growth of wafer-scale graphene using chemical vapor deposition (CVD) and lithographic patterning, large-area graphene nanostructured arrays have been successfully demonstrated by several groups [22], [27]. Graphene's superior electronic and optical properties have raised remarkable interest in high-speed electronics (i.e., graphene-FETs [26]–[28]) and photonic devices (i.e., THz oscillators and low noise sensors [29]). The regime in which graphene's properties are more attractive is located at the transition between electric and photonic sources, in the THz, sub mm-wave range [14], [15].

In this work, we propose and analyze several designs in which graphene may solve the challenge of realizing phase shifters for THz antenna arrays. We consider the propagation properties of subwavelength parallel-plate waveguides (PPWGs) formed by a pair of graphene monolayers with *deeply subwavelength* transverse dimension [Fig. 1(b)] [19]. This graphene PPWG (GPPWG) supports a dominant quasi-TEM mode with no cutoff frequency, similar to metal-insulator-metal (MIM) plasmonic waveguides [Fig. 1(a)] [30]–[32]. Rather strikingly, the guided fields remain confined inside the gap between two *one-atom-thick* graphene monolayers. We apply this geometry to realize novel phase shifter designs, demonstrating that a GPPWG section integrated with *double-gate* (DG) electrodes may enable THz switches and tunable loaded lines, key components to build analog and/or digital phase shifters for antenna applications.

II. Propagation Characteristics of a GPPWG

Graphene is a two-dimensional (2-D) gapless semiconductor composed of a planar atomic layer of carbon atoms [26], with massless and linear energy dispersion near the K, K' points of the Brillouin zone and a Fermi velocity $\nu_F = 10^8$ cm/s. Its surface conductivity may be modeled using the well-known Kubo formula [18]–[20], [23], [24]. In the low THz region, below the interband transition threshold $\hbar\omega = 2|\mu_c|$ ($\hbar$ is the reduced Planck's constant), the electronic intraband transition dominates, the direct interband transition is negligible and $\sigma_s \simeq \sigma_{intra}$. Unique features of ballistic transport and ultrahigh electron mobility (in excess of 20000 $\mathrm{cm^2V^{-1}s^{-1}}$ and weakly dependent on temperature [27]) may characterize graphene as a low-loss atomic-scale conduction surface in this band. The intraband electron-phonon scattering process, mainly depending on impurities and defects, yields [18]–[20]:

$$\sigma_{intra} = -j\frac{e^2 K_B T}{\pi\hbar^2(\omega - j2\Gamma)} \times \left[\frac{\mu_c}{K_B T} + 2\ln\left(e^{-\mu_c/K_B T} + 1\right)\right] \quad (1)$$

where e is the electron charge, K_B is the Boltzmann's constant and Γ is the electron-phonon scattering rate due to the carrier intraband scattering, related to plasmon losses. Here, we assume the temperature $T = 300$ K and $\Gamma = 0.52$ meV [17], [20] consistent with the ballistic transport features of graphene, whose mean free path was measured to be up to 500 nm at room temperature and larger than 4 μm at lower temperatures [18]–[20], [26]–[28]. If $|\mu_c| \gg k_B T$, (1) reduces to the Drude-like expression:

$$\sigma_{intra} = -\frac{je^2\mu_c}{\pi\hbar^2(\omega - j2\Gamma)} \quad (2)$$

where the real part of σ_{intra}, associated with Γ, contributes to energy absorption or dissipation. Fig. 1(b) illustrates the geometry of a GPPWG consisting of two graphene sheets with width w much larger than separation distance d. The propagation axis

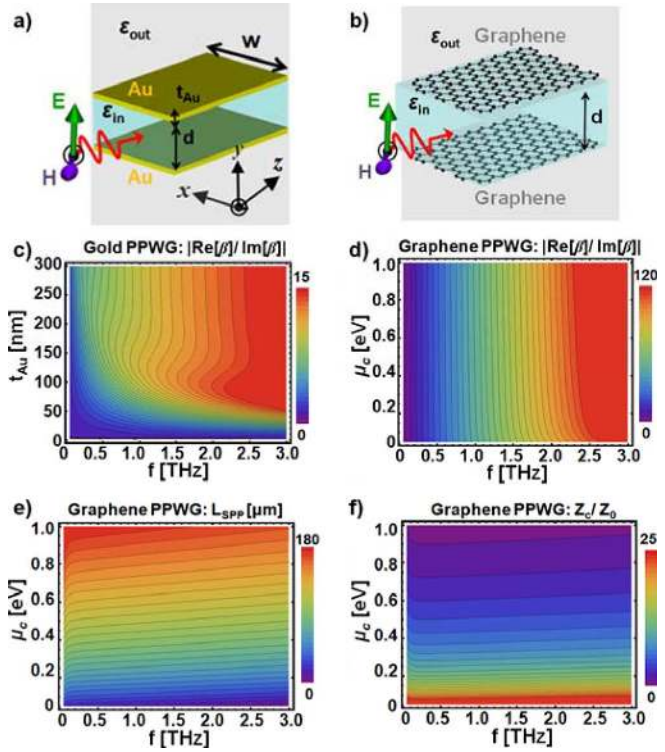

Fig. 1. Schematic diagram of (a) a plasmonic PPWG consisting of a MIM heterostructure (gold-air-gold) and (b) a GPPWG. (c) $|\mathrm{Re}[\beta]/\mathrm{Im}[\beta]|$ (FoM) for the gold PPWG with $d = 300$ nm, varying the frequency f and the gold thickness t_{Au}. (d)–(f) FoM, propagation length, and characteristic impedance normalized to free space for the GPPWGs with $d = 300$ nm, varying frequency and chemical potential μ_c.

is oriented along the z-axis. For TM_z waves with magnetic field $H_x(y)\exp[j(\omega t-\beta z)]$, by forcing a discontinuity on the tangential magnetic field distribution on the graphene surface $\mathbf{J}_s=\hat{y}\times(\mathbf{H}^+-\mathbf{H}^-)=\sigma_s\mathbf{E}$, the complex eigenmodal propagation constant β can be evaluated by solving the dispersion equation:

$$\tanh\left[\frac{\sqrt{\beta^2-\omega^2\mu_0\varepsilon_{\mathrm{in}}}d}{2}\right]\frac{\sqrt{\beta^2-\omega^2\mu_0\varepsilon_{\mathrm{in}}}}{\sqrt{\beta^2-\omega^2\mu_0\varepsilon_{\mathrm{out}}}}=\frac{\varepsilon_{\mathrm{in}}}{-\varepsilon_{\mathrm{out}}+j\frac{\sigma_s}{\omega}\sqrt{\beta^2-\omega^2\mu_0\varepsilon_{\mathrm{out}}}} \quad (3)$$

where $\varepsilon_{\mathrm{in}}$ and $\varepsilon_{\mathrm{out}}$ are the material permittivity inside and outside the waveguide, respectively. When the separation between the graphene monolayers is reduced to a subwavelength scale $d\ll\lambda_0$, the GPPWG supports a quasi-TEM dominant mode [19]. Under the long-wavelength approximation $d\ll\min\left(2\pi/\left|\omega\sqrt{\varepsilon_{\mathrm{in}}\mu_0}\right|,2\pi/\left|\omega\sqrt{\varepsilon_{\mathrm{out}}\mu_0}\right|\right)$ and $\sigma_s\sqrt{\beta^2-\omega^2\mu_0\varepsilon_{\mathrm{in}}}/\omega\varepsilon_{\mathrm{in}}$, $\sigma_s\sqrt{\beta^2-\omega^2\mu_0\varepsilon_{\mathrm{out}}}/\omega\varepsilon_{\mathrm{out}}\gg 1$, a simple approximate explicit dispersion relation can be obtained:

$$\frac{\beta}{k_0}\simeq\sqrt{\frac{\varepsilon_{\mathrm{in}}}{\varepsilon_0}\left(1-j\frac{2}{\omega\mu_0\sigma_s d}\right)}. \quad (4)$$

As expected, for sufficiently large surface conductivity the outer (cladding) permittivity plays a negligible role in tailoring the eigenmodal propagation constant, implying that the mode is tightly confined between the graphene layers. For simplicity, therefore, and without loss of generality, we will assume two suspended graphene sheets in free-space (i.e., $\varepsilon_{\mathrm{in}}=\varepsilon_{\mathrm{out}}=\varepsilon_0$) with same chemical potentials. In many senses, the propagation properties of this waveguide are analogous to the ones of an MIM plasmonic waveguide supporting confined SPP modes.

Here, we specifically define a figure of merit (FoM) for SPP propagation: $|\mathrm{Re}[\beta]/\mathrm{Im}[\beta]|=2L_{SPP}/\lambda_{SPP}$ which can be seen as the propagation length $L_{SPP}=|2\mathrm{Im}(\beta)|^{-1}$ (1/e decay length for power) normalized by the SPP wavelength that is inversely proportional to $\mathrm{Re}[\beta]$. Fig. 1(c) and (d) show contour plots of FoM versus frequency for an MIM PPWG formed by two gold (Au) plates with varying thickness t_{Au}, and a GPPWG with varying chemical potential, where the waveguide height is fixed at $d=0.3\ \mu\mathrm{m}$ in both scenarios and $\varepsilon_{\mathrm{in}}=\varepsilon_{\mathrm{out}}=\varepsilon_0$. The thickness-dependent conductivity of gold is modeled using the Fuchs-Sondheimer (FS) model [33], [34], assuming the gold's mean-free-path to be 20 nm, which yields $\sigma_{3-D}/\sigma_{\mathrm{bulk}}=57.14\%$ for a 10 nm gold nanofilm and $\sigma_{3-D}/\sigma_{\mathrm{bulk}}=97.56\%$ for a 300 nm bulk gold. For gold PPWGs, the optimal guiding property is obtained when gold plates are thicker than 100 nm, which is about the skin depth of bulk gold. It is seen that, despite the extreme thinness of graphene monolayers (~ 0.33 nm), for frequencies higher than 0.5 THz, the GPPWG exhibits a remarkably larger FoM than conventional MIM plasmonic waveguides, i.e., $\mathrm{FoM}=74.48$ is obtained at $f=1.5$ THz for graphene monolayers tuned to $\mu_c=0.5\,\mathrm{eV}$. At the same frequency, a gold PPWG with 300 nm walls has an $\mathrm{FoM}=11.78$. A gold PPWG with wall thickness comparable with graphene would show much poorer waveguiding properties. The impressive FoM of GPPWG is mainly attributed to its strong field localization and good propagation length at THz. Fig. 1(e) shows the propagation length for a GPPWG, as a function of the chemical potential and frequency of operation. A good propagation length is observed, despite coupled SPP waves inside the GPPWG are strongly confined, with a guided wavelength much shorter than the free-space wavelength $\lambda_{\mathrm{SPP}}\ll\lambda_0$ [17], [19], i.e., $L_{SPP}=121.3\ \mu\mathrm{m}$ is obtained at $f=1.5$ THz for a GPPWG tuned to $\mu_c=0.5\,\mathrm{eV}$.

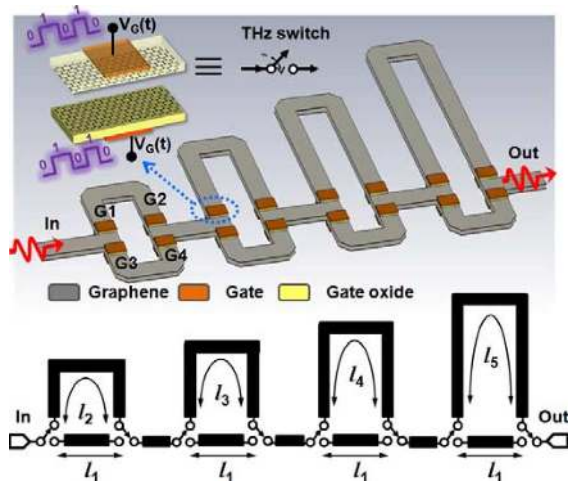

Fig. 2. Schematic diagram (top) and equivalent circuit (bottom) of a digital phase shifter based on graphene transmission lines and switches; here, THz switches are realized combining a GPPWG with a double-gate structure.

In the following, we apply a transmission line model (TLM) and the transfer-matrix method [10], [30] to evaluate the propagation characteristics of integrated waveguide circuits, components and systems embedding GPPWG. We have verified with full-wave simulations that, due to the extreme mode confinement, these analytical tools are very accurate in describing the propagation properties along longitudinally inhomogeneous sections of GPPWG. The modal characteristic impedance may be defined as $Z_c=-E_y/H_x=\beta/\omega\varepsilon_{\mathrm{in}}$ and it is shown in Fig. 1(f), varying the graphene's chemical potential and operating frequency. It is found that propagation constant and characteristic impedance of this transmission-line may be largely tuned from relatively high (i.e., pristine or slightly doped graphene with a small μ_c) to low (heavily doped or strongly biased graphene with large μ_c), which is arguably the most significant advantage of graphene compared to conventional plasmonic waveguides. Having established its remarkable guiding and tunability properties, we envision, in the inset of Fig. 2, a GPPWG combined with a double gate configuration, allowing electronic control and tuning of the propagation constant and local impedance.

Typically, the chemical potential of graphene can be tuned from -1 eV to 1 eV by a modest applied bias [18]–[20]. Due to the electron-hole symmetry in the graphene band structure, both negative and positive signs of chemical potential provide the same complex surface conductivity. The chemical potential of a graphene monolayer, obtained by neglecting the quantum capacitance (i.e., a relatively thick gate oxide), is given by:

$$\mu_c=\hbar v_F\sqrt{\frac{\pi C_{ox}V_g}{e}} \quad (5)$$

where $C_{ox} = \varepsilon_{ox}/t_{ox}$ is the electrostatic gate capacitance, t_{ox} is the thickness of gate oxide and V_g is the applied gate voltage [26]. A double gate consisting of n^+-doped polysilicon or metal gate positioned behind the oxide (i.e., Al_2O_3, SiO_2, BN) [inset of Fig. 2] may simultaneously tune the chemical potential and the associated surface conductivity of top and bottom graphene monolayers. The relationship between chemical potential and bias is discussed in Appendix A. This enables locally varying *in real time* the real part of the propagation constant (associated with phase delay) and the characteristic impedance of the gated segment, with tunability properties shown in Fig. 1.

An important issue to consider is how to couple THz radiation in such thin GPPWGs. A variety of THz sources are currently available, including gyrotron, photomixing devices, and quantum cascade lasers (QCL), to name a few [14], [15]. Semiconductor lasers, i.e., QCL based on intersubband transitions in a multiple repeated quantum-well heterostructures, may have a compact size and are readily integrated in chip-scale THz devices and systems like the ones considered here. The QCL geometry is ideal to couple energy into the transverse mode of a GPPWG and it appears exceptionally suitable to excite the proposed chip-scale graphene phase shifters. Microwave sources followed by multiple stages of harmonic generation can also realize low THz sources. Recently, different groups have proposed compact THz antennas using subwavelength graphene patches [35]. An array of graphene antennas is compatible and integrable with the graphene phase shifters proposed here, and they may be used in the transmitter/receiver front ends to efficiently couple THz radiation from and into free-space.

III. Graphene-Based Phase Shifters

In this section we show how the large FoM and tunability of GPPWGs, described in the previous section, may allow the design of *compact*, *low-loss* and tunable transmission lines in the THz regime. The low-loss features may also allow removing an amplification stage in the transmit/receive (T/R) chain, thus significantly reducing the operating power and system complexity of the beamforming network. In the following, we investigate integrally-gated GPPWGs to realize THz electronic switching devices and active loaded lines for phase shifters. We propose the practical realization of *switched-lines*, *loaded-lines*, and *reflection-type* graphene-based phase shifters [8]–[10].

A. Graphene-Based Digital Phase Shifters

Digital phase shifters (DPS) or switched-line phase shifters are conceptually simple in design. They rely on *true time delay* between two direct transmission line paths (a reference line and a delay line [8], [9]) to provide the desired phase shift. A simple DPS can be built using switched delay-line techniques and single-pole double-throw (SPDT) switches [2], [8]–[10]. By using two SPDT switches, the transmission-line is switched over from one segment to the other, varying the corresponding phase shift [2], [8]–[10]. Fig. 2 shows an example of a 4-bit DPS realized using a cascade of four 1-bit phase shifters (16 switches and 8 different transmission-line segments) with $2^4 = 16$ discrete phase states. For instance, when the switches G1 and G2 are in their ON-state and the switches G3 and G4 are in their OFF-state, the wave will propagate in the delay line l_2. By switching the signal between l_1 and l_2, it is possible to realize an increase in the phase shift $\Delta\phi = \beta\Delta l$, where $\Delta l = l_2 - l_1$ is the difference between the physical length of the delay and reference lines. By using the proper combination of ON/OFF-states, one can in principle implement any discrete number of phase states between 0° and 360°.

Electronic switches are widely used in conventional antenna systems for time-multiplexing, time-division multiple access, pulse modulation and channel switch in receiver or transmit/receive (T/R) modules. In practical high-frequency DPS designs, the most crucial issue consists in realizing stable and high-speed switches that can replace conventional RF diodes or FETs. Graphene active transmission lines may offer a robust approach to translate such switching devices at THz. The main idea is to integrate a GPPWG with a double gate, as shown in the top panel of Fig. 2. By controlling V_g, we may vary the chemical potential of the gated graphene segment, affecting the phase velocity, characteristic impedance, propagation constant and associated phase shift along each gated GPPWG segment [as observed in Fig. 1(f)]. We can use this property to tune the transmission characteristics through the gated section with an external bias.

We consider two designs to realize graphene-based THz switches in order to achieve the desired voltage-controlled switching operation. As a first design, by using chemical doping, we tailor the chemical potential of the ungated graphene sections to be much larger than the gated line in the unbiased state, producing significant impedance mismatch and large reflection at the interface between gated and ungated sections. This scenario corresponds to the OFF-state of the switch. Since the chemical potential may be largely tuned by applying a gate voltage, it is possible to pass from OFF to ON-state by properly biasing the gated section, effectively lowering its impedance until matching the outer line.

Consider, for instance, a GPPWG made of doped graphene with $\mu_c = 0.5$ eV. In the gated section, graphene monolayers with low chemical potential $\mu_c = 0.025$ eV are considered to realize switches operating at $f_0 = 0.6/1.2/2.5$ THz. The gate length is assumed to be one quarter of the guided wavelength of the gated line, with values $l = 0.77\ \mu\text{m}$ ($f_0 = 2.5$ THz), $l = 1.74\ \mu\text{m}$ ($f_0 = 1.2$ THz), and $l = 3.55\ \mu\text{m}$ ($f_0 = 0.6$ THz). These lengths are much shorter than the free-space wavelength, thanks to the large value of $\text{Re}(\beta)$ associated with SPP propagation, providing a significant benefit for device scaling and compatibility with on-chip technology. Fig. 3(a) shows the reflection coefficient versus gated chemical potential for this THz switch at the different design frequencies. It is observed that in the OFF-state, without any applied bias $\mu_c = 0.025$ eV, the reflection is extremely high. However, when the gated sections are biased to $\mu_c = 0.5$ eV, complete transmission is obtained. This operation is rather independent of the frequency of operation in the considered range of frequencies. Fig. 3(b) shows the corresponding bandwidth of operation for different values of chemical potential, confirming the large operational bandwidth of this device.

As an alternative design, we consider graphene switches based on Fabry-Perot tunneling. Here, we assume the chemical potential of the ungated and gated sections to be $\mu_c = 0.025$ eV

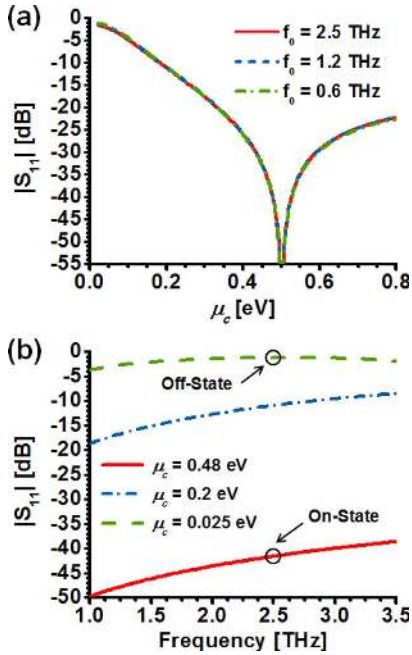

Fig. 3. (a) Magnitude of the reflection coefficient versus chemical potential for THz switches as in Fig. 2. Here, heavily-doped and low-doped graphene sections are used for the ungated and gated sections, respectively. The ON-state is realized by impedance matching the gated and ungated transmission-line segments. (b) Magnitude of the reflection coefficient versus frequency, varying the chemical potential in the gated section.

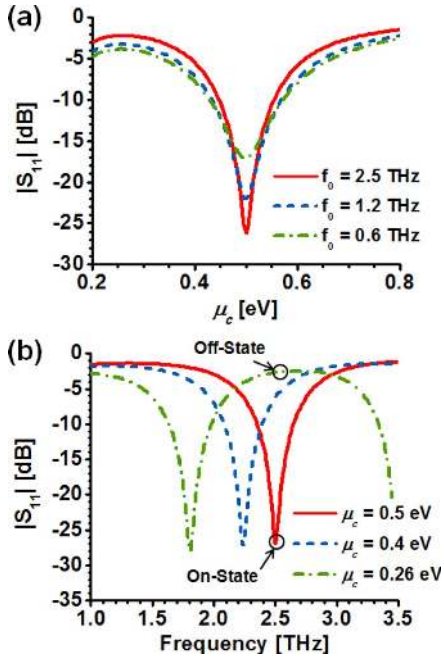

Fig. 4. (a) Magnitude of the reflection coefficient versus chemical potential for THz switches, as in Fig. 2. Here, low-doped and moderately-doped graphene sections are used for the ungated and gated section, respectively. The ON-state is realized based on Fabry-Perot resonant tunnelling. (b) Magnitude of the reflection coefficient versus frequency, varying the chemical potential in the gated section.

and $\mu_c = 0.3$ eV, respectively. The ON-state is now achieved by biasing the gate to $\mu_c = 0.5$ eV. In this case, we exploit the wavelength dispersion of the SPP mode and design the gate length to be half of the guided wavelength for $\mu_c = 0.5$ eV. The gate lengths are $l = 6.05$ μm at $f_0 = 2.5$ THz, $l = 12.85$ μm at $f_0 = 1.2$ THz and $l = 25.90$ μm at $f_0 = 0.6$ THz. Fig. 4(a) shows the corresponding reflection coefficient versus chemical potential of the gated sections. In the OFF-state, without bias, very high reflection is obtained, but when the gated sections are biased to $\mu_c = 0.5$ eV, complete transmission is achieved, due to the drastic change in β that yields to $\beta l = \pi$. Fig. 4(b) shows that the reflection of this switch is more sensitive to the level of chemical potential compared to the previous nonresonant design. This design may be however more interesting for narrow-band filtering and sensing applications.

Before concluding this section, we should mention that, according to Fig. 1(d), the ungated sections employed in these designs are necessarily more lossy than the doped sections. Even without bias, however, the line shows a rather high FoM $=$ 55.88 at 1.5 THz, ensuring that insertion loss is reasonable, as it has also been confirmed by our numerical results. Both presented designs may hold great potential to realize switching devices in THz integrated photonic and optoelectronic circuits.

B. Graphene-Based Loaded-Line Phase Shifters

The basic principle of a loaded-line phase shifter (LLPS) can be illustrated with the circuit in the bottom panel of Fig. 5, in which a loaded-line produces a specific phase variation $\Delta\phi = \beta l$ [10]. In practical designs, insertion and return losses are inherently present in this design, due to reflections at the mismatched loaded-line. At RF and microwaves, a LLPS is usually realized by loading a transmission-line with two shunt susceptances and separation length $\lambda/4$ [10]. In the THz regime, we may realize a graphene-based LLPS using the configuration shown in Fig. 5, consisting of a double gate with length $l_p = 7.5$ μm. The chemical potential of the gated and ungated lines are 0.0685 eV and 0.5 eV, respectively. By electrically tuning the chemical potential of the gated line, we can adjust the phase shift in real time, ideally covering a wide range of phase shifts. Unfortunately, the bias will also affect the characteristic impedance of the gated section, introducing unwanted reflections due to impedance mismatch. Fig. 6(a)–(c) show the S-parameters and phase shifts of the LLPS in Fig. 5 designed to realize phase delays of 90°/180°/270°/360° at the operating frequency $f_0 = 1.5$ THz. In order to achieve the desired phase delays, the chemical potential of the gated section is biased to

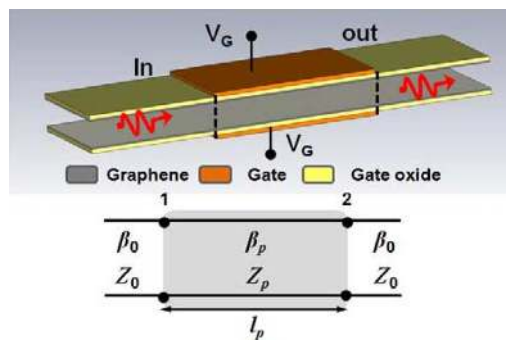

Fig. 5. Schematic diagram (top) and equivalent circuit (bottom) of a graphene-based loaded-line phase shifter, which allows a wide range of phase shift at the price of possibly larger reflection (or return loss) compared to the design of Fig. 2.

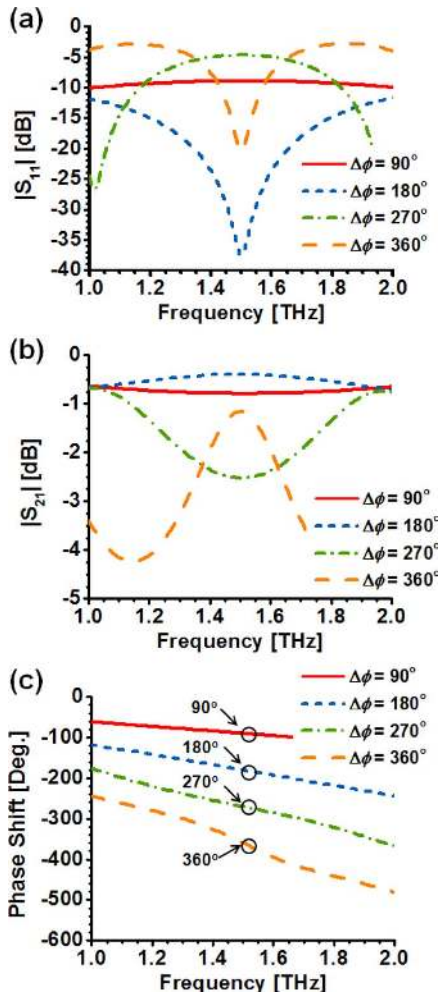

Fig. 6. (a) Magnitude of reflection and (b) transmission coefficients, (c) phase difference between input and output ports of the graphene-based load-line phase shifter in Fig. 5.

$\mu_c = 1.072/0.272/0.124/0.0685$ eV, respectively. Even if the desired phase shift is indeed obtained, as verified in Fig. 6(c), we find relatively large reflections when the amount of phase shift is $\Delta\phi = (2m-1)\pi/2$, where m is an integer, i.e., for $\Delta\phi = 90°$ and 270°, as the impedance of gated and ungated lines are significantly mismatched. Impedance transformation sections may be necessary to eliminate the reflection.

In order to solve this issue, we propose a tunable matching network consisting of a multistage gated GPPWG. Fig. 7 shows the schematic diagram and circuit model of the dynamic-matching LLPS design. The gate G6, with the longest gate length, is used to generate the desired phase shift by biasing the graphene layers. In order to match the complex impedance at the input of G6, we need two additional gated sections. By properly biasing G5, zero reactance can be obtained at the input of G5 (point y in Fig. 7). We further need a $\lambda/4$ transformer to match the real part of the input impedance at point x in Fig. 7. This may be obtained by tuning l_q, corresponding to the gated region covered by the other four gates in Fig. 7, as a quarter of the guided wavelength, and bias the section to have a characteristic impedance equal to:

$$\mathrm{Re}\left[Z_q\right] = \sqrt{\mathrm{Re}\left[Z_0\right]\mathrm{Re}\left[Z_{in,y}\right]} \tag{6}$$

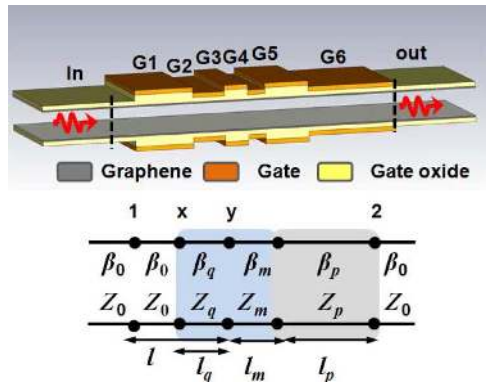

Fig. 7. Schematic diagram (top) and equivalent circuit (bottom) of a loaded-line phase shifter with a dynamic matching transformer. This design can ensure a lower reflection compared to Fig. 5.

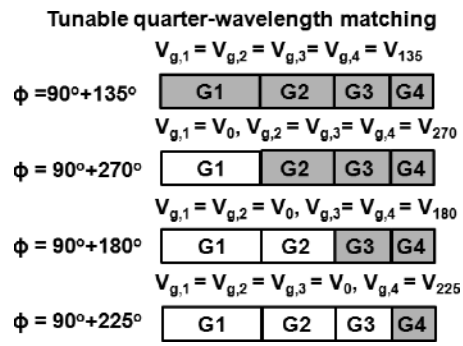

Fig. 8. Operation principle of the dynamically tunable quarter-wavelength transformer in Fig. 7.

where Z_0 and $Z_{in,y}$ are the impedance of the ungated lines and the input impedance at point y, respectively.

To operate the phase shifter, we need to be able to tune the desired phase shift $\Delta\phi$, which is obtained by changing β_p and the corresponding bias parameters. In addition, we need to be able to dynamically adjust the line length l_q, which is effectively modified when different biases are applied. This is obtained by discretizing the $\lambda/4$—line into multiple stages, controlled by four consecutive gates G1, G2, G3 and G4, as shown in Fig. 7. This cascade of gates effectively forms a dynamic matching network, as illustrated in Fig. 8.

Consider, for instance, an absolute phase variation $\Delta\phi = 90 + 135°$ (additional 90° is caused by the signal propagation through the $\lambda/4$—transformer). In this case, we apply equal voltages to all four gates in the transformer section (G1, G2, G3, G4), such that they possess the same characteristic impedance (6), and the sum of their lengths is equal to the electric length $l_q = \lambda_q/4$ at the design frequency. When a phase variation $\Delta\phi = 90 + 225°$ is desired, only G4 should be biased, which provides the required characteristic impedance and electrical length (i.e., l_q is now the gate length of G4 only). An arbitrary phase variation $\Delta\phi$ may be obtained by solving the coupled system at the design frequency:

$$\begin{cases} \Delta\phi = \mathrm{Re}[\beta_p]l_p + \mathrm{Re}[\beta_m]l_m + \mathrm{Re}[\beta_q]l_q + \mathrm{Re}[\beta_0]\left(l - l_q\right) \\ \mathrm{Im}[Z_{in,y}] = 0 \\ \mathrm{Re}[Z_q] = \sqrt{\mathrm{Re}[Z_0]\mathrm{Re}[Z_{in,y}]} \\ \mathrm{Re}[\beta_q]l_q = \frac{\pi}{2} \end{cases} \tag{7}$$

TABLE I
DESIGN PARAMETERS OF A DYNAMICALLY MATCHED LLPS

	$\mu_{c,p}$ [eV]	$\mu_{c,m}$ [eV]	$\mu_{c,q}$ [eV]	l_q [μm]
$\Delta\phi = 90 + 135°$	0.701	0.625	0.678	5.97
$\Delta\phi = 90 + 180°$	0.428	0.396	0.421	4.69
$\Delta\phi = 90 + 225°$	0.306	0.185	0.281	3.82
$\Delta\phi = 90 + 270°$	0.0685	0.378	0.587	5.55

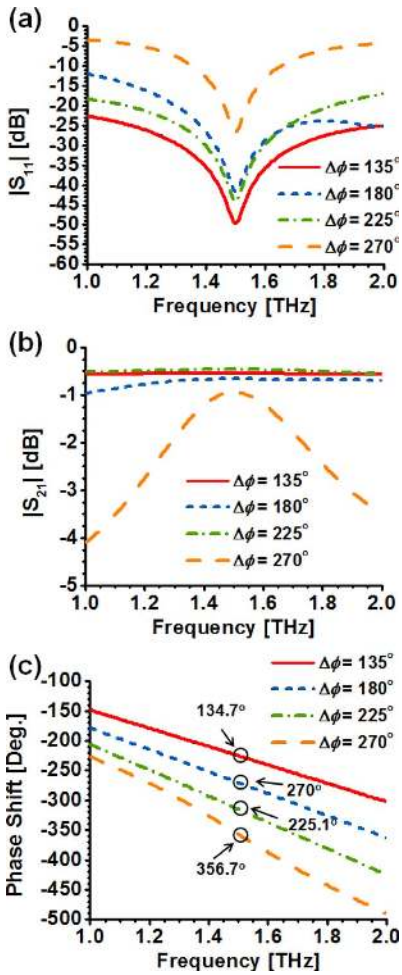

Fig. 9. (a) Magnitude of reflection and (b) transmission coefficients and (c) phase difference between input and output ports for the load-line phase shifter shown in Fig. 8.

As an example of a practical LLPS design, we consider $l_p = 3.6\ \mu\text{m}$, $l_m = 1.8\ \mu\text{m}$, $l = 9\ \mu\text{m}$ and a chemical potential for the ungated and gated lines of 0.5 eV and 0.0685 eV, respectively. By solving (7), the optimal values of β_p, β_m and l_q, as well as of the required chemical potential in each section, are obtained to achieve the desired phase variations $\Delta\phi = 90 + 135/180/225/270°$. The optimal design parameters are found in Table I.

Fig. 9(a)–(c) show the reflection and transmission coefficients and absolute phase shift for this LLPS design, confirming optimal performance at the design frequency $f_0 = 1.5$ THz. Very low insertion loss and a phase error below $\pm 3\%$ is obtained for all cases. The residual phase error and insertion loss are due to graphene losses. This LLPS design with tunable matching network may provide dynamic matching and it eliminates reflections due to impedance mismatch, which may be of interest in smart antenna systems, i.e., frequency division multiple access (FDMA) devices that require tunable sub mm-wave antennas with band-selection and dynamic matching.

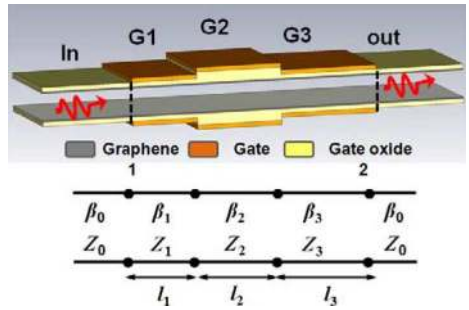

Fig. 10. Schematic diagram (top) and equivalent circuit (bottom) of a simplified digital (3-bit) loaded-line phase shifter.

For most phased-array applications, we are mostly concerned with the *relative* phase shift between different ports, rather than its absolute value. In Fig. 10, we propose a simplified LLPS design, consisting of a 3-bit phase shifter with 8 phase shift states: 0/45/90/135/225/270/315°. We assume a chemical potential of 0.05 eV for both gated and ungated graphene segments. In order to minimize reflections, when gate voltages are applied we set the length of each loaded section to be a multiple of half guided wavelength. The characteristic impedance and propagation constant of the ungated sections are given by (Z_0, β_0) The loaded lines are characterized by (Z_1, β_1), (Z_2, β_2) and (Z_3, β_3). If we intend to create impedance matching for all binary states, the following requirements for the "i"-th section need to be fulfilled:

$$\begin{cases} \beta_i l_i = \pi \\ \beta_0 l_i - \beta_i l_i = \Delta\phi_i \end{cases} \tag{8}$$

where $\Delta\phi$ is defined as the relative phase shift between the unbiased and biased conditions for the i-th section and the total phase shift is $\Delta\phi = \Delta\phi_1 + \Delta\phi_2 + \Delta\phi_3$. For a design with phase shifts of 45° (bit 0), 90° (bit 1) and 180° (bit 2), the required chemical potentials are $\mu_{c,1} = 0.085$ eV (bit 0), $\mu_{c,2} = 0.122$ eV (bit 1), and $\mu_{c,3} = 0.213$ eV (bit 2), and the associated optimal gate lengths are: $l_1 = 4.13\ \mu\text{m}$, $l_1 = 4.96\ \mu\text{m}$, and $l_1 = 6.62\ \mu\text{m}$. We may generate 8 different states through electronically programmable gate voltage signals in this configuration. Fig. 11 shows numerical results for the corresponding S parameters and phase shifts for this design. Very low reflection and nearly unitary transmission are obtained, with the desired relative phase shifts at the operating frequency $f_0 = 1.5$ THz. This simplified LLPS design may facilitate the implementation of THz phased-arrays with digital beam forming and steering functions.

C. Graphene-Based Analog Phase Shifters

In addition to the binary phase shifts discussed above, analog phase shifters (APS) are commonly implemented in RF systems, for applications when the phase shift should be continuously controlled by a bias with almost unlimited resolution [8]–[10]. To realize a graphene-based THz APS, we need to design an electrically-adjustable reactive circuit element that may provide

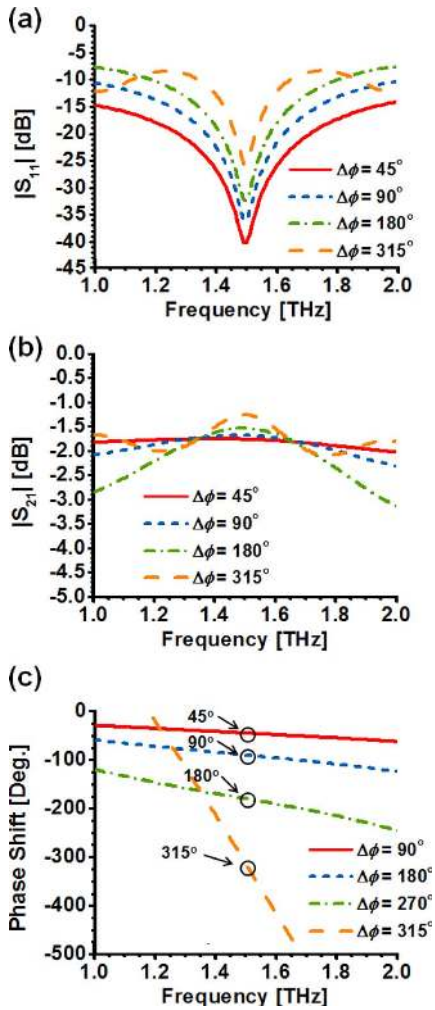

Fig. 11. (a) Magnitude of reflection and (b) transmission coefficients and (c) phase difference between input and output ports for the load-line phase shifter shown in Fig. 10.

analog phase shifts. In [21], we have demonstrated electronic frequency tuning of a cloaking device at THz frequencies using a graphene monolayer. It is possible to use the same concept to make a variable inductor by inserting a vertically-aligned graphene monolayer into the GPPWG, as shown in Fig. 12. By choosing a $d_{s.c.} = \lambda/4$ distance from a ground plane, we achieve a tunable inductive load X_s, schematically indicated in the circuit model of Fig. 12. In this design, we assume the graphene chemical potential to be set at 0.5 eV.

Fig. 13 shows the numerical results for the phase shift as a function of chemical potential at the operating frequency $f_0 = 2.5$ THz varying the distance between G1 (switch) and G2 (IR variable inductor). By adjusting the bias voltage at G2, the inductive reactance in the equivalent circuit of Fig. 12 is tuned, in turn analogically controlling the overall phase shift over a wide angular range. Fig. 14 shows the phase shift versus frequency for a graphene-based APS with $l = 4$ μm. At the operating frequency $f_0 = 3$ THz, phase shifts ranging from $-124.2°$ to $-213.5°$ can be obtained, when the chemical potential of the vertically-gated graphene is biased from 0.01 eV to 0.5 eV. It is interesting that the tuning range increases for larger frequencies. The proposed APS design may achieve moderate phase shift

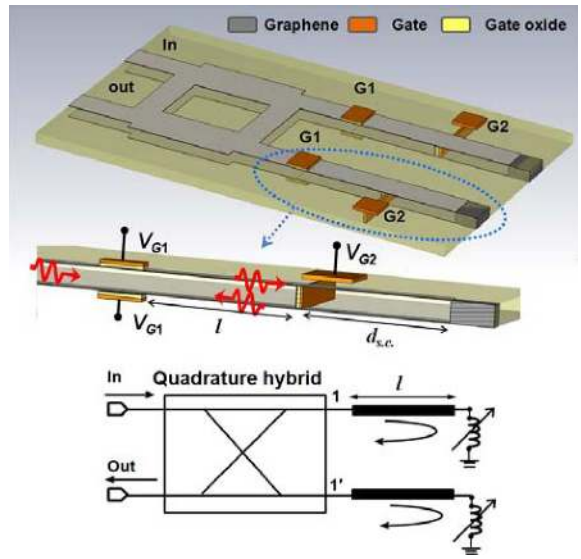

Fig. 12. Schematic diagram (top) and equivalent circuit (bottom) of a reflection-type analog phase shifter.

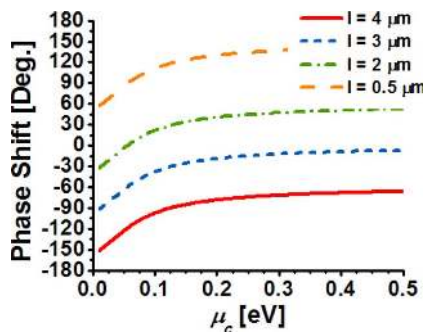

Fig. 13. Phase difference between input and output ports for the analog phase shifter of Fig. 12.

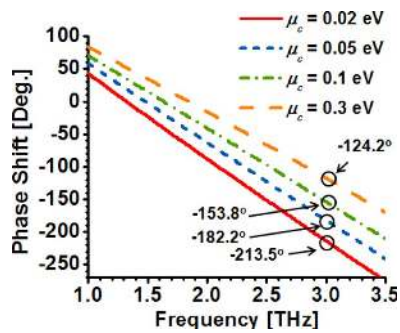

Fig. 14. Variation of the phase difference between input and output ports versus the frequency for the analog phase shifter of Fig. 12, varying the chemical potential of the vertically-aligned graphene monolayer.

and high resolution with fewer active components than DPS, but at the cost of increased fabrication difficulty due to the vertically-aligned graphene monolayer.

IV. Conclusions

We have proposed, here, a variety of phase shifter designs for operation in THz phased arrays, based on double-gated graphene parallel-plate waveguides. By using graphene-based switches, loaded-line and/or variable inductors, three types of

phase shifters, with wide phase shift range, have been proposed in the THz range. Due to the strong SPP wave localization of graphene-based waveguides, it is possible to realize low-loss, compact on-chip switching and phase control devices. In addition, these functions may be electronically programmed by applying bias signals at the double gate. We believe that the proposed phase shifters may be used in the near future in phased-array antennas, beamforming networks, phase discriminators, and vector modulators for THz communication and sensing systems.

APPENDIX

For an electrically gated graphene sheet with oxide thickness t_{ox}, a variation in the chemical potential is equivalent to a voltage drop V_{ch} across the quantum capacitance C_Q [36], [37]:

$$V_{ch} = \frac{\mu_c}{e} = \frac{C_{ES}}{C_{ES} + \frac{1}{2}C_Q(V_g)} V_g \tag{A1}$$

where the quantum capacitance C_Q, related to the difference between the electron and hole sheet densities (n and p [cm^{-2}]), can be expressed as:

$$\begin{aligned} C_Q &= e\frac{\partial(p-n)}{\partial V_{ch}} \\ &= \frac{2e^2 K_B T}{\pi(\hbar v_F)^2} \ln\left[2\left(1+\cosh\frac{eV_{ch}}{K_B T}\right)\right] \end{aligned} \tag{A2}$$

and the conventional electrostatic capacitance is:

$$C_{ES} = \frac{\varepsilon_{ox}}{t_{ox}}. \tag{A3}$$

Hence, (A1) may be solved self-consistently to evaluate the relationship between chemical potential and gate voltage for different gate oxide thickness. Since the overall sheet charge density in the graphene $Q_{sh} = e \times (p-n) = \int C_Q dV_{ch} = (1/2)C_Q V_{ch}$ shows a specific dependency on V_{ch}, one would expect that only its half value is used in (A1), consistent with [37]. In general, for relative thick gate oxide, $C_{ES} \ll C_Q$ is valid, and an explicit expression of chemical potential for moderately doped graphene, i.e., $|\mu_c| \gg K_B T$, may be derived, as (5) [20], [21], [37]). In some cases, C_{ES} could be larger than C_Q, due to the finite density of states of graphene. This occurs only when either the value of ε_{ox} is extremely high or the gate oxide is ultrathin (i.e., few nm). In the extreme case of $C_{ES} \gg C_Q$ the chemical potential is almost directly responsible for the applied gate voltage, i.e., $\mu_c/e \approx V_g$.

REFERENCES

[1] D. M. Pozar and D. H. Schaubert, *Microstrip Antennas: The Analysis and Design of Microstrip Antennas and Arrays*. New York, NY, USA: IEEE Press, 1995.

[2] K. Chang, *RF and Microwave Wireless System*. New York, NY, USA: Wiley, 2000.

[3] D. Parker and D. C. Zimmermann, "Phased arrays—part II: Implementations, applications, and future trends," *IEEE Trans. Microwave Theory Tech.*, vol. 50, pp. 688–698, 2002.

[4] M. A. Antoniades and G. V. Eleftheriades, "Compact linear lead/lag metamaterial phase shifters for broadband applications," *IEEE Antennas Wireless Propag. Lett.*, vol. 2, pp. 103–106, 2003.

[5] F. Ellinger, "Varactor-loaded transmission-line phase shifter at C-band using lumped elements," *IEEE Trans. Microwave Theory Tech.*, vol. 51, pp. 1135–1140, 2003.

[6] X. Guan, H. Hashemi, and A. Hajimiri, "A fully integrated 24-GHz eight-element phased-array receiver in silicon," *IEEE J. Solid-State Circuits*, vol. 39, pp. 2311–2320, 2004.

[7] G. M. Rebeiz, G. L. Tan, and J. S. Hayden, "RF MEMS phase shifters: Design and applications," *IEEE Microwave Mag.*, vol. 3, pp. 72–81, 2002.

[8] L. G. Maloratsky, "Electrically tunable switched-line diode phase shifters Part 1: Design procedure," *High Freq. Electron.*, pp. 16–21, May 2010.

[9] L. G. Maloratsky, "Electrically tunable switched-line diode phase shifters Part 2: Multisection circuits," *High Freq. Electron.*, pp. 60–67, May 2010.

[10] D. M. Pozar, *Microwave Engineering*, 2nd ed. New York, NY, USA: Wiley, 1998.

[11] F. Schwierz and J. J. Liou, *Modern Microwave Transistors: Theory, Design, and Performance*. New York, NY, USA: Wiley, 2002.

[12] C. F. Hsieh, R. P. Pan, T. T. Tang, H. L. Chen, and C.-L. Pan, "Voltage-controlled liquid-crystal terahertz phase shifter and quarter-wave plate," *Opt. Lett.*, vol. 31, pp. 1112–1114, 2006.

[13] H. T. Chen, W. J. Padilla, M. J. Cich, A. K. Azad, R. D. Averitt, and A. J. Taylor, "A metamaterial solid- state terahertz phase modulator," *Nat. Photon.*, vol. 3, pp. 148–151, 2009.

[14] M. J. Fitch and R. Osiander, "Terahertz waves for communications and sensing," *John Hopkins APL Tech. Digest*, vol. 25, pp. 348–354, 2004.

[15] J. Federici and L. Moeller, "Review of terahertz and subterahertz wireless communications," *J. Appl. Phys.*, vol. 107, pp. 111101–111101, 2010.

[16] A. Alù and N. Engheta, "Wireless at nanoscale: Optical interconnects using matched nanoantennas," *Phys. Rev. Lett.*, vol. 104, pp. 213902–213902, 2010.

[17] A. Vakil and N. Engheta, "Transformation optics using graphene," *Science*, vol. 332, pp. 1291–1294, 2011.

[18] G. W. Hanson, "Dyadic Green's functions and guided surface waves for a surface conductivity model of graphene," *J. Appl. Phys.*, vol. 103, pp. 064302–064302, 2006.

[19] G. W. Hanson, "Quasi-transverse electromagnetic modes supported by a graphene parallel-plate waveguide," *J. Appl. Phys.*, vol. 104, pp. 084314–084314, 2008.

[20] G. W. Hanson, "Dyadic Green's functions for an anisotropic, non-local model of biased graphene," *IEEE Trans. Antenna Propag.*, vol. 56, pp. 747–757, 2008.

[21] P. Y. Chen and A. Alù, "Atomically thin surface cloak using graphene monolayers," *ACS Nano*, vol. 5, pp. 5855–5863, 2011.

[22] L. Ju, B. Geng, J. Horng, C. Girit, M. Martin, Z. Hao, H. A. Bechtel, X. Liang, A. Zettl, Y. R. Shen, and F. Wang, *Nat. Nanotech.*, vol. 6, pp. 630–634, 2011.

[23] V. P. Gusynin, S. G. Sharapov, and J. P. Carbotte, "Magneto-optical conductivity in graphene," *J. Phys.: Cond. Mater.*, vol. 19, pp. 026222–026222, 2007.

[24] L. A. Falkovsky and S. S. Pershoguba, "Optical far-infrared properties of a graphene monolayer and multilayer," *Phys. Rev. B*, vol. 76, pp. 153410–153410, 2007.

[25] F. T. Chuang, P. Y. Chen, T. C. Cheng, C. H. Chien, and B. J. Li, "Improved field emission properties of thiolated multi-wall carbon nanotubes on a flexible carbon cloth substrate," *Nanotech.*, vol. 18, pp. 395702–395702, 2007.

[26] K. S. Novoselov, A. K. Geim, S. V. Morozov, D. Jiang, Y. Zhang, S. V. Dubonos, I. V. Grigorieva, and A. A. Firsov, "Electric field effect in atomically thin carbon films," *Science*, vol. 306, pp. 666–669, 2004.

[27] A. K. Geim and K. S. Novoselov, "The rise of graphene," *Nat. Mater.*, vol. 6, pp. 183–191, 2007.

[28] A. H. C. Neto, F. Guinea, N. M. R. Peres, K. S. Novoselov, and A. K. Geim, "The electronic properties of graphene," *Rev. Mod. Phys.*, vol. 81, pp. 109–162, 2009.

[29] F. Rana, "Graphene terahertz plasmon oscillators," *IEEE Trans. Nanotech.*, vol. 7, pp. 91–99, 2008.

[30] S. E. Kocabas, G. Veronis, D. A. B. Miller, and S. Fan, "Transmission line and equivalent circuit models for plasmonic waveguide components," *IEEE Quan. Electron.*, vol. 14, pp. 1462–1472, 2008.

[31] A. Pannipitiya, I. D. Rukhlenko, M. Premaratne, H. T. Hattori, and G. P. Agrawal, "Improved transmission model for metal-dielectric-metal plasmonic waveguides with stub structure," *Opt. Express*, vol. 18, pp. 6191–6204, 2010.

[32] A. Alù and N. Engheta, "Optical nano-transmission lines: Synthesis of planar left-handed metamaterials in the infrared and visible regimes," *J. Opt. Soc. Am. B*, vol. 23, pp. 571–583, 2006.

[33] K. Fuchs, "The conductivity of thin metallic films according to the electron theory of metals," *Proc. Cambridge Philos. Soc.*, vol. 34, pp. 100–108, 1938.
[34] J. Vancea, G. Reiss, and H. Hoffmann, "Mean-free-path concept in polycrystalline metals," *Phys. Rev. B*, vol. 35, pp. 6435–6437, 1987.
[35] I. Llatser, C. Kremers, A. Cabellos-Aparicio, J. M. Jornet, E. Alarcon, and D. N. Chigrin, "Graphene-based nano-patch antenna for terahertz radiation," *Photon. Nanostruct: Fundam. Appl.*, 2012, to be published.
[36] T. Fang, A. Konar, H. Xiang, and D. Jena, "Carrier statistics and quantum capacitance of graphene sheets and ribbons," *Appl. Phys. Lett.*, vol. 91, pp. 092109–092109, 2007.
[37] S. A. Thiele, J. A. Schaefer, and F. Schwierz, "Modeling of graphene metal-oxide-semiconductor field-effect transistors with gapless large-area graphene channels," *J. Appl. Phys.*, vol. 107, pp. 094505–094505, 2010.

Pai-Yen Chen (S'09) was born in Taiwan on September 19, 1982. He received both the B.S. and M.S. degrees in mechanical engineering (major) and electro-optical engineering from the National Chiao Tung University, Taiwan, in 2004 and 2006, respectively.

From 2006 to 2009, he was an Assistant Researcher at the National Nano Device Laboratories (NDL), Taiwan. Since 2009, he has been working toward the Ph.D. degree at the University of Texas at Austin, Austin, TX, USA. His doctoral work focuses mainly on nonlinear, passive and active electromagnetic metamaterials and plasmonics, and their RF, THz, infrared and optical applications. He is also actively engaged on graphene and carbon-based nanoelectronics and nanophotonics. He has published over 60 refereed papers in peer-reviewed journals and conference proceedings, and one book chapter on these topics.

Mr. Chen was officially nominated as the Chinese Phi Tau Phi honorable member in 2006. He was the recipient of the United Microelectronics Corp. (UMC) Scholarship in 2005, finalist and honorable mention Student Contest Award at IEEE Antennas and Propagation Symposium in 2010 and 2011, respectively, Study Aboard Award from Taiwan Ministry of Education in 2010, 3rd prize Student Contest Award in Metamaterials Congress in 2011, 3rd prize Student Contest Award in USNC-URSI National Radio Science Meeting in 2012, and the Donald D. Harrington Dissertation Fellowship from University of Texas at Austin in 2012.

Christos Argyropoulos (S'04–M'11) received the Diploma of Electrical and Computer Engineering from the Aristotle University of Thessaloniki, Greece (2006). He holds an M.Sc. degree in communication engineering from the University of Manchester, U.K. (2007), and the Ph.D. degree in electronic engineering from Queen Mary, University of London, U.K. (2010).

He is currently a Postdoctoral Fellow in the Metamaterials and Plasmonics Laboratory, Department of Electrical and Computer Engineering, University of Texas at Austin, Austin, TX, USA.

He has published over 70 technical papers in highly ranked journals and refereed conference proceedings, including two book chapters. Some of the papers have been published in *Physical Review Letters, Optics Express, Physical Review A/B/E, New Journal of Physics, Applied Physics Letters, Journal of Optical Society of America B*, and the IEEE TRANSACTIONS ON ANTENNAS AND PROPAGATION. His main research interests include computational electromagnetics, numerical and analytical modeling of metamaterials and their applications, antenna design and UWB systems, transformation optics, linear and nonlinear plasmonics, active metamaterials, thermal emission from plasmonic structures, graphene nanophotonics and novel energy harvesting devices.

Dr. Argyropoulos is a Member of the IEEE Antennas and Propagation Society, IEEE Communications Society, SPIE, Optical Society of America, American Physical Society and the Technical Chamber of Greece. He has received several travel and research awards, such as an EPSRC Research Scholarship, the Royal Academy of Engineering international travel grant and was twice awarded the Marie Curie Actions Grant to attend the European School of Antennas. He has given invited talks and seminars to different conferences and university institutions.

Andrea Alù (S'03–M'07–SM'12) received the Laurea, M.S., and Ph.D. degrees from the University of Roma Tre, Rome, Italy, in 2001, 2003, and 2007, respectively.

Currently, he is an Assistant Professor at the University of Texas at Austin. From 2002 to 2008, he was working periodically at the University of Pennsylvania, Philadelphia, PA, USA, where he also developed significant parts of his Ph.D. and postgraduate research. After spending one year as a Postdoctoral Research Fellow at UPenn, in 2009 he joined the faculty of the University of Texas at Austin. He is also a member of the Applied Research Laboratories and of the Wireless Networking and Communications Group at UT Austin. He is the coauthor of over 180 journal papers and 20 book chapters, with over 3800 citations to date. He has organized and chaired various special sessions in international symposia and conferences. His current research interests span over a broad range of areas, including metamaterials and plasmonics, electromagnetics, optics and photonics, scattering, cloaking and transparency, nanocircuits and nanostructures modeling, miniaturized antennas and nanoantennas, RF antennas and circuits.

Dr. Alù is a full member of URSI and a senior member of OSA and SPIE. He is currently an Associate Editor of the *IEEE Antennas and Wireless Propagation Letters*, *Optics Express*, *Metamaterials* and of *Advanced Electromagnetics*. He has guest edited special issues in the *IEEE Journal of Selected Topics in Quantum Electronics*, *Optics Communications*, *Metamaterials* and *Sensors* on a variety of topics involving metamaterials, plasmonics, optics and electromagnetic theory. Over the last few years, he has received several research awards, including the OSA Adolph Lomb Medal (2013), the URSI Issac Koga Gold Medal (2011), the SPIE Early Career Investigator Award (2012), an NSF CAREER award (2010), the AFOSR Young Investigator Award (2010) and the DTRA Young Investigator Award (2011), the Leopold B. Felsen Award for Excellence in Electrodynamics (2008), Young Scientist Awards from URSI General Assembly (2005), and URSI Commission B (2010, 2007 and 2004). His students have also received several awards, including student paper awards at the IEEE Antennas and Propagation Symposia (in 2011 to Y. Zhao, in 2012 to J. Soric). He has been serving as OSA Traveling Lecturer since 2010 and as the IEEE joint AP-S and MTT-S chapter chair for Central Texas.